

Abstractive Representation and Exploration of Hierarchically Clustered Diffusion Tensor Fiber Tracts

Weri Chen ^{†1} Song Zhang ^{‡2} Stephfan Correia ^{§3} David S. Ebert ^{¶4}

¹State Key Lab of CAD&CG, Zhejiang University, ²Mississippi State University, ³Brown University, ⁴Purdue University

Abstract

Diffusion tensor imaging (DTI) has been used to generate fibrous structures in both brain white matter and muscles. Fiber clustering groups the DTI fibers into spatially and anatomically related tracts. As an increasing number of fiber clustering methods have been recently developed, it is important to display, compare, and explore the clustering results efficiently and effectively. In this paper, we present an anatomical visualization technique that reduces the geometric complexity of the fiber tracts and emphasizes the high-level structures. Beginning with a volumetric diffusion tensor image, we first construct a hierarchical clustering representation of the fiber bundles. These bundles are then reformulated into a 3D multi-valued volume data. We then build a set of geometric hulls and principal fibers to approximate the shape and orientation of each fiber bundle. By simultaneously visualizing the geometric hulls, individual fibers, and other data sets such as fractional anisotropy, the overall shape of the fiber tracts are highlighted, while preserving the fibrous details. A rater with expert knowledge of white matter structure has evaluated the resulting interactive illustration and confirmed the improvement over straightforward DTI fiber tract visualization.

Categories and Subject Descriptors (according to ACM CCS): I.3.7 [Computer Graphics]: Three-Dimensional graphics and realism I.3.5 [Computer Graphics]: Curve, surface, solid, and object representations

1. Motivation

Water molecules in biological tissue engage in apparently random Brownian motion or water diffusion. This diffusion process is constrained by the structures in the biological tissues such as neural fibers or muscle fibers. Therefore, it is possible to reconstruct these fibrous anatomical structures from the diffusion information. With an MRI scanner, diffusion information from biological tissues can be gathered *in vivo* in the form of the diffusion tensors [BML94].

Tractography methods reconstruct fibrous structures such as neural fibers in the human brain from the DTI

data [BPP*00]. However, overly dense fiber models can appear visually cluttered thereby impeding identification of specific tracts of interest. Fiber clustering techniques have been developed to overcome this problem by bundling the spatially and anatomically related DTI fibers into tracts [OW05, MMH*05]. These tracts are identified by neuroscientists as representing anatomical structures with high probability [ZCL08]. While the clustering methods group the fibers into meaningful bundles with their own boundaries, their display can still suffer from visual clutter which may impede the selection of specific fiber structures. Recognition of specific fiber tracts can also be hindered by the lack of visual boundaries between them.

To address these problems, we seek to simplify the fiber tracts by focusing on the location, shape, and connectivity of the major anatomical structures. We reduce the complexity of the fiber models in three aspects. First, the fibers are hierarchically grouped into a set of bundles with a proximity-based clustering algorithm. Second, for each fiber tract, we

[†] chenwei@cad.zju.edu.cn. This work was done while Wei Chen was a visiting scholar at Purdue university.

[‡] szhang@cse.msstate.edu. Wei Chen and Song Zhang have identical technical contributions.

[§] stephen_correia@brown.edu

[¶] eberrd@purdue.edu

build an approximate geometric shape and generate a set of principal fibers that are used to depict the overall shape and orientation of the tract. Our third scheme is an interactive multi-valued volume illustration system, which allows the users to choose the appropriate level in the hierarchy, the clusters and the models to display. Rather than using standard geometric rendering, we employ volume rendering to display the mixed scene. One main reason is that many interesting features are contained in a volume data, e.g., the property volume. It would be straightforward and effective to directly visualize it using volume rendering. Meanwhile, converting geometric lines into a volume data would make the entire rendering pipeline seamless. Although fibers can be displayed as polygon models, representing fibers with a volume data makes the performance independent of the number of fibers. Interactive volumetric exploration through the data provides both a comprehensive view to understand the global layout of the fiber tracts and the fiber tract geometry, as well as the local properties such as the individual fiber connectivity. Figure 1 shows our visualization results of a normal human brain with unclustered DTI fibers, clustered DTI fibers, geometric hulls and geometric hulls with principal fibers inside. Based on our results, a neuropsychologist can easily make an annotation (Figure 1 (d)).

2. Related Work

Diffusion Tensor Imaging Visualization A wide range of methods have been developed in the last decade for DTI visualization [JH04, WH06, PB07]. The DTI fibers encode the direction of fastest diffusion in the tensor field and also convey the connectivity information, which is important for anatomical studies. These fibers are shown to correlate with fibrous structures in the biological tissues [SHWF98]. Recently developed fiber clustering methods group the DTI fibers into the fiber tracts based on some similarity measure between the fibers [MVW05]. Different clustering methods have been applied, such as spectral clustering [BKP*04] and hierarchical clustering [ZCL08]. DTI fibers have been visualized with both surface model [ZDL03] and volume rendering [WKZL04]. When the fiber density is high, DTI fiber visualization can suffer from visual cluttering which makes it difficult to readily identify specific tracts of interest and slows down the user interaction. Accordingly, efforts have been made to generate evenly-spaced DTI fibers [VBvP04, MSE*05], wrap groups of DTI fibers into hulls [ESM*05], and accelerate the fiber display rendering with graphics hardware [PFK07, MSE*06].

This paper aims to provide effective representation and interaction of the DTI fibers. Our work on the geometric hull is similar to the one introduced by Enders *et al.* [ESM*05]. However, the geometric hull we proposed is generated directly from the DTI fibers instead of from a center line and a set of boundary curves, thus avoiding assumptions on the geometry of the fiber bundles. The purpose of the principal

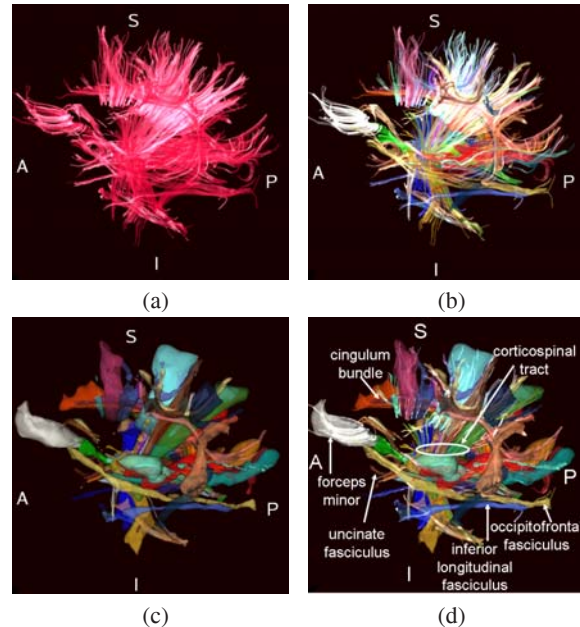


Figure 1: Visualization of the DTI fibers of a normal human brain with (a) unclustered DTI fibers, (b) clustered DTI fibers, (c) geometric hulls, and (d) geometric hulls with principal fibers inside. (d) was annotated by a neuropsychologist. A: Anterior; P: Posterior; S: Superior; I: Inferior.

curves is to capture the needed level of abstraction, which is different from the goal of the evenly-spaced streamline methods. Our results show that the principal curves complements the geometric hull by providing details on fiber bundle orientation while limiting visual cluttering. In summary, our approach aims to alleviate the visual cluttering problem by focusing on illustrating the main features of the fiber tracts while providing sufficient details and context.

Scientific Illustration The main goal of scientific illustration is to communicate information effectively using a painting or image by highlighting important features while suppressing insignificant details. In terms of the data source, previous work can be roughly classified into two categories. The first one directly visualizes a measured data set without changing the data set itself [ER02]. To simulate the appearances of certain artistic styles or concepts, some approaches make full use of transparency and texture [Int97], visibility [CSC06], or object deformation [CLE07]. The second category is designed to artificially generate an additional data set using different techniques. For instance, Schussman and Ma [SM04] proposed to sample the illumination of lines into an anisotropic voxel representation based on spherical harmonics for depicting extremely dense and thin line data. Weiskopf and his colleagues [WSE07] employed appearance texture to illustrate the line structure of an unsteady 3D flow. Other researchers explored topology [STS07], line

pattern [Int97], surface [GIS03], or solid texture [LE05] to convey the information in a measured data set efficiently. General solutions for visualizing the fiber tracts represent the fiber connectivity with simple geometry like streamlines or streamtubes. Our approach advances this simplification by introducing both a hierarchical organization for fibers and a shape approximation to each clustered bundle.

3. Data

A Siemens Symphony 1.5T scanner was used for imaging. Three slice packets of diffusion-weighted images were acquired sagittally and interleaved to acquire a data volume of $128 \times 128 \times 90$ with a voxel size of $1.7 \times 1.7 \times 1.7$ mm. This data is then scaled to a volume of $256 \times 256 \times 180$ with a voxel size of $0.85 \times 0.85 \times 0.85$ mm. The Siemens MDDW protocol was used, with two b values (0, 1000) in 12 directions. Diffusion tensor images were calculated.

DTI fibers were generated by uniformly seeding in the data volume with a high seeding density of $1/0.85\text{mm}^3$ and jittering in order to cover the entire data volume without aliasing artifacts. The DTI fibers were then culled to remove those that were too similar to others (distance threshold = 0.85 mm, minimum distance threshold = 0.475 mm) [ZDL03]. We used two data sets in this paper. They generated 7,223 and 2,406 fibers respectively.

4. Method

We first construct a hierarchical clustering of fiber bundles (Section 4.1). These bundles are then reformulated into a 3D multi-valued volume data, which provides a hierarchical abstraction of the input diffusion tensor image. We also build a set of geometric hulls in Section 4.2 and principal fibers (Section 4.3) to approximate the shape and orientation of each fiber bundle. We then merge the hierarchical clustering model, the geometric hulls, the principal curves, and other data volume into a single display volume (Section 4.4). By simultaneously visualizing and exploring the multi-valued volume data, the geometric hulls and other property volumes (Section 4.5), the overall shape of the fiber tracts are highlighted, while preserving the fibrous details.

4.1. Hierarchical Clustering

The DTI fibers for each subject were clustered using a modified single-linkage algorithm [ZCL08]. The distance between two fibers A and B was defined as a thresholded average distance: $D(A, B, t) = \max(d(A, B, t), d(B, A, t))$, where $d(A, B, t) = \text{mean}_{a \in A, \min_{b \in B} \|a - b\| > t} \min_{b \in B} \|a - b\|$, and a and b are evenly spaced sample points on A and B .

The single-linkage algorithm produced a hierarchy of clusters. The hierarchy was then cut at different levels with different clustering distance thresholds. Lower distance threshold produces more and smaller clusters: higher distance threshold produces less and bigger clusters. Compared to some optimization-based algorithms such as spectral clustering methods [BKP*04], single-linkage algorithm

ensures a minimum distance threshold between clusters and the hierarchical structure of the clusters naturally assists the exploration of the clustering results at the different levels-of-abstraction. These clusters can then be visualized with geometric hulls (Section 4.2) and principal fibers (Section 4.3).

Figure 2 shows four levels on the hierarchy generated from the first data set with polygonal rendering. Some anatomical structures such as the cingulum bundles (indicated by yellow arrows) are clearly visible and distinct from other fibers in (c), but are broken into multiple bundles in (a), (b), and merged with other anatomical bundles in (d).

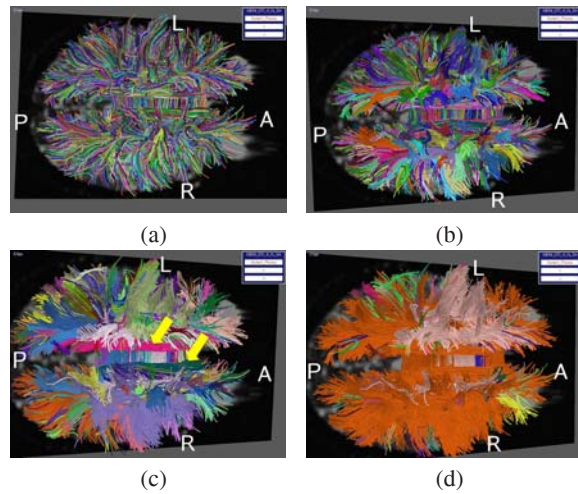


Figure 2: The hierarchical clustering results on the first data set with the distance thresholds at (a) 0.5 mm, (b) 2.0 mm, (c) 4.0 mm, and (d) 5.0 mm. The left and right cingulum bundles are shown with yellow arrows in (c).

4.2. Smoothed Geometric Hulls

For each cluster, we collect all vertices and build a geometric hull by means of the alpha shape algorithm [EM94]. An alpha shape is a concrete geometric object that is uniquely defined for a particular point set. Given a finite point set and an alpha, the alpha shape of the point set is a polytope, which is neither necessarily convex nor necessarily connected. The alpha value of zero leads to a geometric hull that tightly bounds a point set. We construct such a geometric hull for each fiber cluster and represent it as a triangle model due to two reasons. One on hand, the concept of alpha shapes formalizes the intuitive notion of shape for spatial point set data, and is especially suitable for the point sets of fibers. On the other hand, alpha shapes are generalizations of the convex hull, and can approximate concave objects.

The geometric hull effectively represents the shape of the fiber bundle and provides a rough sense to the size and shape of the underlying fiber bundle. Due to the complexity of the vertex distribution of the fiber bundles, the geometry of the

built hull is ill-defined, as shown in Figure 3 (b). In practice, we employ the Poisson surface reconstruction technique [KBH06] to refine the hull. We first densely sample the boundary of the alpha shape hull into a set of points associated with their normals. The point set is then used as a guidance field to reconstruct a smooth triangle model within given accuracy (Figure 3 (c)).

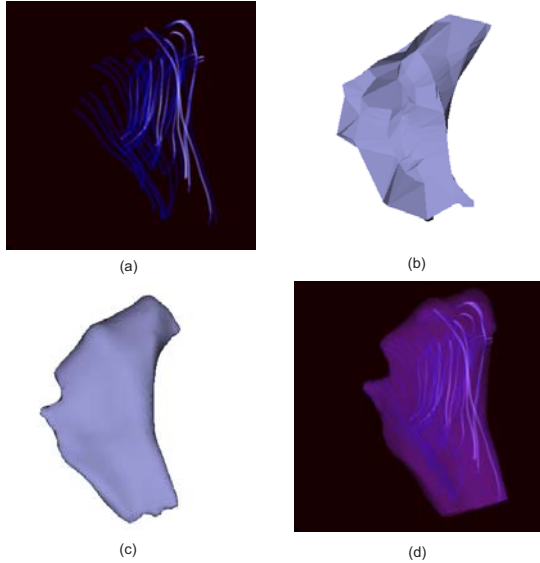


Figure 3: (a) A fiber cluster; (b) The geometric hull of the fiber bundle; (c) The refined hull with Poisson reconstruction technique; (d) The composition of the refined hull and the fiber bundle. (b) and (c) are rendered with polygonal models.

4.3. Principal Fiber Tracts

Expressive visual exploration requires efficient abstraction of the underlying data. Because the tracked fibers are densely located and in a limited space, it is quite difficult to have a clear picture of the entire fiber cluster structures without careful investigation. On the other hand, although the geometric hulls can be used to simplify the fiber bundles, they do not indicate the spatial orientations of the fiber bundles in many situations. Therefore, an additional shape proxy for abstracting the complex fiber bundles is required.

Our solution is to compute one or several principal fiber tracts for constructing a canonical representation of all tracts within a fiber bundle. We assume that all fiber tracts within the bundle $\{C_1, C_2, \dots, C_m\}$ are independent and identically distributed samples from a smooth principal fiber tract $C = f(\lambda)$ parametrized by $\lambda \in [0, 1]$. More specifically, each tract C_i represented by a sequence of vertices $\{V_i^j\}$ is generated from the following generative model:

- (1) Sample two values λ_i^B and λ_i^E uniformly from $[0, 1]$, without loss of generality, $\lambda_i^B < \lambda_i^E$.

- (2) Denote n_i as the vertex number of C_i and pick it to be proportional to the arc length of C_i , i.e., $n_i = c(\lambda_i^E - \lambda_i^B)$ for certain constant c .
- (3) For $j = 1, 2, \dots, n_i$: $V_i^j = f(\lambda_i^j) + \varepsilon_i^j$, where $\lambda_i^1 = \lambda_i^B$, $\lambda_i^{n_i} = \lambda_i^E$, $\{\lambda_i^j, j = 2, \dots, n_i - 1\}$ is a set of different values that are uniformly distributed over $(\lambda_i^1, \lambda_i^{n_i})$, and ε_i^j are independent identically distributed samples from the normal distribution with mean 0 and variance $\sigma^2 I$.

Without any assumption of the parametric form of f , we propose to estimate f with a modified principal curve algorithm. The standard principal curve algorithm [HTF01] extracts a dominant curve from a set of points by computing the parameters of f . It can not be applied to a group of curves because it handles the problem on the basis of points and do not consider the line length. Instead, we regard a set of points belonging to a curve as a group, and only estimate the λ values for two end points, compute the λ values for the rest of points based on the arc length. The new algorithm is stated as two iterative steps:

$$\hat{f}(\lambda) \leftarrow E(V_i^j | \lambda(V_i^j) = \lambda) \quad (1)$$

$$\hat{\lambda}_f(V_i^j) \leftarrow \arg \min_{\lambda'} \|V_i^j - \hat{f}(\lambda')\|^2 \quad j = 1, n_i \quad (2)$$

$$\hat{\lambda}_f(V_i^j) = \ell_i^j / \ell_i \left(\hat{\lambda}_f(V_i^{n_i}) - \hat{\lambda}_f(V_i^1) \right) \quad j = 2, \dots, n_i - 1$$

where E denotes the expectation, ℓ_i is the arc length of C_i , and ℓ_i^j is the arc length from the first vertex to V_i^j . Equation (1) is known as the self-consistency property, which states that $f(\lambda)$ is the average of all points that have the parameter value λ . The first formula of Equation (2) computes the λ values for two end points of the underlying curve. The λ values of other points are estimated with the second formula of Equation (2).

Similar to standard principal curve algorithm, the modified algorithm presented in Equations 1 and 2 has no guarantee of global optimality, and the estimator \hat{f} is sensitive to its initial value. In simple cases where all fiber tracts in a bundle are similarly oriented, the first principal component would be a good choice (Figure 4 (a)). However, a bundle may contain fibers that can be visually distinguished into two or more sub-sets (Figure 4 (b)). Such complicated structures may not be captured by a simple principal fiber.

Intuitively, this problem can be partially solved by using a local version of the above technique to find a principal tract for every local region. Note that the low hierarchies of the hierarchical clustering structure are generated with a small threshold, and it is reasonable to assume that the fiber tracts of each fiber bundle in the low hierarchies have the similar orientation and can be represented by one principal fiber tract. Therefore, we first build a principal fiber tract for each cluster in an appropriately low hierarchy (in our case, the third hierarchy). For each of the higher hierarchies, we then simply unite the principal fibers of its child nodes as its principal fiber tracts. In summary, the algorithm for computing the principal fiber tracts is as follows:

- 1: For adequately low hierarchies, build a principal fiber tract for each cluster with the modified algorithm.
- 2: For each cluster of each higher hierarchy (e.g., from the third to the highest hierarchy), employ the principal fiber tracts of its child nodes as its principal fiber tracts.
- 3: For each principal fiber tract of each cluster, find its nearest fiber tract on the cluster and use it to represent the principal fiber tract.
- 4: For each principal tract, assign a special identification.

The third step of this Algorithm yields an approximated principal fiber tract that is one of the input fiber tracts. This scheme avoids adding additional fiber tracts to the initial fiber tracts. The identification produced in the fourth step is used to generate a compact multi-valued volume as described in Section 4.4. Figure 4 (d) illustrates our results for fiber bundles in three consecutive hierarchies.

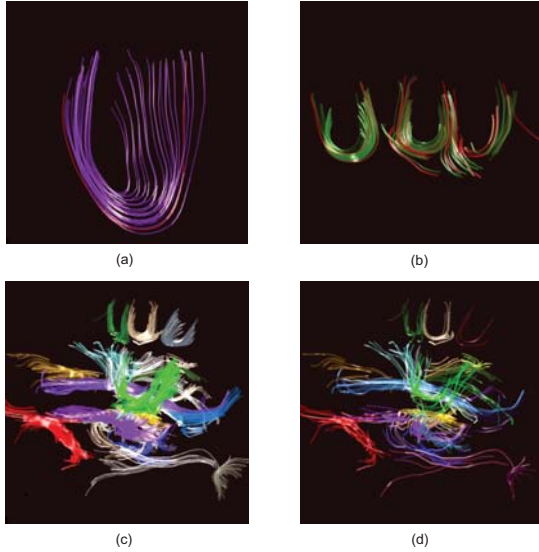


Figure 4: (a) Fiber tracts with similar orientation (the principal fiber tract is shown in red); (b) Fiber tracts with distinguishable orientations (the principal fiber tracts are shown in red); (c) Several fiber bundles; (d) Hierarchical computation for principal fiber tracts.

4.4. The Multi-Valued Volume

We build the multi-valued volume based on the hierarchical clustered fiber model, which acts as the structural guidance. The volume has the same or larger resolution as that of the input DTI data. Similar to [WKZL04], we voxelize each fiber into a list of voxels using the 3D Bresenham algorithm and filter the distances from each voxel to the fiber tract with a 3D Gaussian kernel, which spans two or three voxels. The filtered distance d and the direction vector \vec{v} of each fiber play the same roles as the density and gradient in a standard volume rendering algorithm as they provide the shape and lighting information respectively. Thus, they are the primary values stored in the multi-valued volume.

The third value recorded in the multi-valued volume is the cluster identification s of each fiber tract, which will be used to identify different clusters during visual exploration. For each hierarchy, we can generate a multi-valued volume. To encode the principal fiber tracts in the entire hierarchical clustered model, we do not generate a volume for every hierarchy. Instead, we represent all fiber tracts in a multi-valued volume and identify the principal fiber tracts as an integer l . This value is first initialized as zero for each fiber tract. We assign each hierarchy h with an integer 2^h and check the status of each fiber. If the i th fiber is the principal fiber tract of certain hierarchy h , we accumulate the corresponding integer 2^h to its identification l_i . Typically, the maximum hierarchy of a hierarchical clustering model is 8, and we can use an unsigned char to encode this identification.

Other associated properties of the input DTI image can be packed into the multi-valued volume, such as the T2-weighted data from which we can distinguish between water, white matter, and air regions, or the fractional anisotropic data that records the anisotropy of each data point. Table 1 summarizes the encoded values.

Property	Format
The filtered distance, d	1 byte
The direction of the tracts, \vec{v}	3 bytes
The magnitude of the tract direction, g	1 byte
The cluster of each tract, s	2 bytes
The principal fiber tract identification, l	1 byte
The T2-weighted image of each voxel (optional)	1 byte
The fractional anisotropy of each voxel (optional)	1 byte

Table 1: The encoded information in the multi-valued volume

4.5. Visual Exploration of the Multi-Valued Volume

We encode the resulting multi-valued volume with two or three four-channel volume textures. To display the geometric hulls, and the volume within a pipeline, we design a two-phase algorithm. In the first stage, we peel the geometric hulls into a list of depth layers [Eve01] under given lighting and viewpoint. The depth and color information of all layers are encoded as two sets of textures, whose sizes are the same as that of the frame buffer. The second stage renders the multi-valued volume with a 3D texture-slicing algorithm. For each fragment rasterized from each slice, we compare its depth with the depth stored in each geometric layer. If the current slice is the nearest one to the layer, we composite the color from the geometric layer with that of the multi-valued volume. In this way, the contributions from all geometric layers are orderly composed with the multi-valued volume. Figure 5 demonstrates the advantage of this scheme with a phantom fiber model and six geometric models.

The popular illumination model for delineating the line structures is the one proposed in [Ban94]:

$$C = k_a + C_l(k_d(\sqrt[m]{1 - (\vec{v} \cdot \vec{L})^2}) + k_s(\sqrt[m]{1 - (\vec{v} \cdot \vec{H})^2})), \alpha = \alpha_l \quad (3)$$

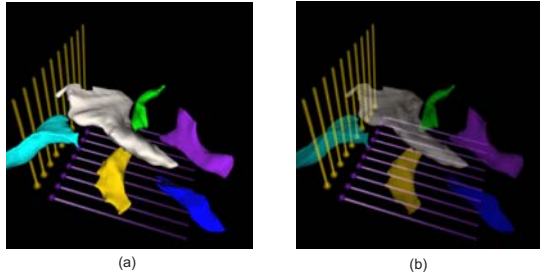


Figure 5: (a) Order-false result; (b) Order-correct result.

where k_a , k_d , and k_s are the coefficients for ambient, diffuse, and specular components. (C_t, α_t) is the color and opacity determined from the user-adjustable 2D transfer function that is dependent on the density and gradient magnitude. Three vectors \vec{v} , \vec{L} , and \vec{H} are the fiber tract direction, the light direction, and the halfway vector between the lighting and viewing directions. m and n denote the excess-brightness diffuse and shininess exponents respectively.

To flexibly depict the used-selected clusters and the principal fiber tracts in the given hierarchy, we modify the line illumination model presented in Equation 3 as follows:

$$C = \text{sgn}(l - l_u)(k_a + C_s(k_d(\sqrt[m]{1 - (\vec{v} \cdot \vec{L})^2}) + k_s(\sqrt[n]{1 - (\vec{v} \cdot \vec{H})^2})))$$

$$\alpha = \alpha_s, \alpha_t \quad (4)$$

where (C_s, α_s) denotes adjustable color and opacity of the cluster s , to which the current fragment belongs. l is the principal fiber tract identification of the underlying fragment, and $l_u = 2^{h_u}$ is an integer computed from the user-specified hierarchy h_u . The function $\text{sgn}(l - l_u)$ is used to display the principal fiber tracts of the selected hierarchy.

Figure 6 compares the effects between the standard Banks model and our scheme. It is apparent that clarifying clusters with different colors greatly facilitates the discrimination among different clusters. Thus, our approach is superior to the method proposed by Wenger *et al.* [WKZL04], which can only offer the effect with Equation 3. In addition, by comparing a sequence of multi-valued volumes that are generated with different hierarchies, we can gain a rough idea on the hierarchical cluster structure, as demonstrated in Figure 6 (b-d). For example, the left and right cingulum bundles (identified by the yellow arrows in Figure 6 (a)) are broken into multiple pieces in Figure 6 (b). They are approximately grouped into two distinct fiber bundles in Figure 6 (c), and are merged into one fiber bundle in Figure 6 (d).

For other property volumes, their contributions are mixed with those from the fiber tracts and the geometric hulls in the fragment level. We adopt the traditional volume illumination model to illuminate them:

$$C = k_a + C_t(k_d(\vec{N} \cdot \vec{L}) + k_s((\vec{N} \cdot \vec{H})^n)), \quad \alpha = \alpha_t \quad (5)$$

where \vec{N} denotes the gradient vector.



Figure 6: (a) Rendering the fiber bundles (2,406 fibers) of the multi-valued volume using the Banks model (Equation 3); (b-d) The results with the modified model (Equation 4). All tracts are displayed (i.e., l_u is set to be zero). The hierarchies for (b-d) are 6, 8, and 9 separately.

5. Results

We have implemented the proposed approach on a PC with an Intel 2.2 GHz CPU, 1.5G RAM and nVidia Geforce 8800 video card. The entire visualization pipeline was implemented with NVidia Cg shader model 4.0.

A neuropsychologist with strong knowledge of white matter architecture evaluated our results. We asked him to try to identify the layout, shape, orientation, and fibrous details of the fiber tracts that correlate with the brain anatomy. He observed the unclustered DTI fibers, the clustered DTI fibers, the geometric hulls, and the geometric hulls with principal curves. With unclustered DTI fibers, he was able to identify the orientation of the brain and the layout of large white matter fiber tracts such as the cingulum bundles, parts of the corpus callosum, and a few other larger bundles such as the forceps minor that stand out from their surrounding bundles due to their location and trajectory. However, he had trouble discriminating between other fiber bundles, especially those with partly adjacent trajectories (e.g., inferior longitudinal and occipitofrontal fasciculus). With clustered DTI fibers, he was able to identify more fiber tracts that correlate with the brain anatomy; however, the visual clutter from crowded fibers often hindered the identification of the overall shape and boundary of the tracts. With geometric hulls and principal curves presentation, he was able to identify the overall layout and shapes of the fiber tracts with greater ease, and at the same time he was able to identify the orientation of

the individual tracts. He also noted that the increased speed of interaction over the previous DTI fiber visualization helps getting more perspectives on the model and facilitates the recognition of the anatomical structures. He used our visualization to annotate some fiber tracts in Figure 1 (d).

Due to the video memory limitation, we set the resolution of the multi-valued volume as 256^3 . For a fundamental configuration (Table 1), each voxel consumes 8 bytes, leading to a total amount of 128 M bytes. The memory consumption for each depth layer is approximately 2 M bytes. Generally, four layers are appropriate for displaying all geometric hulls. The rendering performance is heavily dependent on the number of slices and the depth layers. The geometric hulls have to be rendered multiple times in the first stage to extract all layers. Note that this extraction only happens when the viewing or lighting configuration is changed. With a frame buffer resolution of 500×500 and the texture slicing number of 1,000, the average performance is around 2 fps.

Figure 7 shows the results using geometric hulls for the second data set. The left image solely depicts all hulls at a given hierarchy level (with distance threshold at 3.6 mm), while the right one mixes the principal fiber tracts to enhance the perception to the orientation of the clusters.

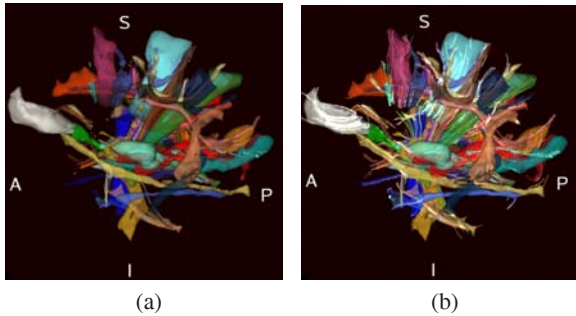


Figure 7: The abstractive visualization of the fiber tracts using (a) geometric hulls only, and (b) geometric hulls with principal fibers inside. The first data set was used.

When we selectively combine the geometric hulls, the fiber tracts, and an anisotropy volume, the multi-valued volume visualization provides a comprehensive visualization and interactive analysis experience. Figure 8 demonstrates the results. Anatomical features such as the cingulum bundles, inferior longitudinal fasciculus, and the U-fibers are identified by a neuropsychologist in the picture.

Our approach shares the similar idea of [WKZL04] for representing the fibers with a volume with two significant differences. First, we employ a robust hierarchical clustering approach to give the volume a schematic classification. The identification information can be used to enhance the visualization with different coloring schemes for the background and the fiber bundles. The jump among different hierarchies benefits the understanding of the global cluster structure.

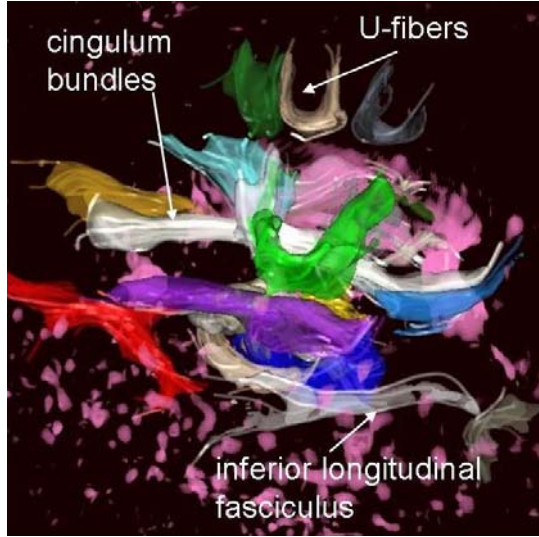


Figure 8: The comprehensive visualization of the fiber tracts with geometric hulls, principal fibers, and the fractional anisotropy volume. The second data set was used.

Second, we create an abstractive representation with geometric hulls and principal curves, which greatly reduces the complexities of the input DTI volume data set.

6. Conclusions

In this paper we introduce methods for simplifying and abstracting complicated DTI fiber tracts toward achieving an insightful illustration of these tracts. A neuropsychologist evaluated the system, and the results indicate that the abstraction of the fiber tracts as well as the multi-valued volume provides a potentially valuable tool for better understanding the white-matter anatomy from these tracts. This work can benefit hypotheses testing about the cognitive and behavioral correlates of white-matter tracts in both healthy and diseased brains.

In the future, we expect to explore more abstraction techniques. The current solution for computing principal fiber tracts only works for simple fiber bundle. We plan to design a more robust algorithm for extracting multiple principal fiber tracts from a complex fiber bundle.

7. Acknowledgements

We would like to thank Nvidia for equipment donations. W. Chen is supported by NSF of China (No. 60503056). S. Zhang and S. Correia are supported by the NOAA Northern Gulf Cooperative Institute (NA06OAR4320264 06111039), the Research Initiation Program, Mississippi State University, the NIA PAR-03-056, the Alzheimer's Association (NIRG-03-6195), and the Ittleson Fund, Brown University.

D. Ebert is supported by NSF Grants 0081581, 0121288, 0328984, and the U.S. Department of Homeland Security.

References

- [Ban94] BANKS D. C.: Illumination in diverse codimensions. In *Proceedings of ACM SIGGRAPH* (1994), pp. 327–334.
- [BKP*04] BRUN A., KNUTSSON H., PARK H.-J., SHENTON M., WESTIN C.-F.: Clustering fiber traces using normalized cuts. In *MICCAI* (2004), pp. 368–375.
- [BML94] BASSER P., MATTIELLO J., LEBIHAN D.: Estimation of the effective self-diffusion tensor from the NMR spin echo. *Journal of Magnetic Resonance, Series B* 103, 3 (March 1994), 247–54.
- [BPP*00] BASSER P. J., PAJEVIC S., PIERPAOLI C., DUDA J., ALDROUBI A.: In vivo fiber tractography using DT-MRI data. *Magnetic Resonance in Medicine* 44 (2000), 625–632.
- [CLE07] CHEN W., LU A., EBERT D. S.: Shape-aware volume illustration. *Computer Graphics Forum (Special Issue of Proceedings of Eurographics)* 27, 3 (2007), 705–714.
- [CSC06] CORREA C., SILVER D., CHEN M.: Feature-aligned volume manipulation for illustration and visualization. *IEEE Transactions on Visualization and Computer Graphics* 12, 5 (2006), 1069–1076.
- [EM94] EDELSBRUNNER H., MÜCKE E. P.: Three-dimensional alpha shapes. *ACM Transactions on Graphics* 13, 1 (1994), 43–72.
- [ER02] EBERT D., RHEINGANS P.: Volume illustration: Non-photorealistic rendering of volume models. In *Proceedings of IEEE Visualization* (Boston, USA, October 2002), pp. 253–264.
- [ESM*05] ENDERS F., SAUBER N., MERHOF D., HASTREITER P., NIMSKY C., STAMMINGER M.: Visualization of white matter tracts with wrapped streamlines. In *Proceedings of IEEE Visualization 2005* (2005), pp. 51–58.
- [Eve01] EVERITT C.: Interactive order-independent transparency. *Interactive order-independent transparency. Technical report, NVIDIA Corporation.* (May 2001).
- [GIS03] GORLA G., INTERRANTE V., SAPIRO G.: Texture synthesis for 3D shape representation. *IEEE Transactions on Visualization and Computer Graphics* 9, 4 (2003), 512–524.
- [HTF01] HASTIE T., TIBSHIRANI R., FRIEDMAN J.: *The Elements of Statistical Learning: Data Mining, Inference, and Prediction.* Springer Verlag, 2001.
- [Int97] INTERRANTE V.: Illustrating surface shape in volume data via principal direction-driven 3D line integral convolution. In *Proceedings of ACM SIGGRAPH* (1997), pp. 109–116.
- [JH04] JOHNSON C. R., HANSEN C. D.: *Visualization Handbook.* Academic Press, June 2004.
- [KBH06] KAZHDAN M., BOLITHO M., HOPPE H.: Poisson surface reconstruction. In *Proceedings of the Fourth Eurographics Symposium on Geometry Processing* (2006), pp. 61–70.
- [LE05] LU A., EBERT D.: Example-based volume illustrations. In *Proceedings of IEEE Visualization* (2005), pp. 655–662.
- [MMH*05] MADDAM M., MEWES A. U. J., HAKER S., GRIMSON W. E. L., WARFIELD S. K.: Automated atlas-based clustering of white matter fiber tracts from DTMRI. In *MICCAI* (2005).
- [MSE*05] MERHOF D., SONNTAG M., ENDERS F., HASTREITER V. P., FAHLBUSCH R., NIMSKY C., GREINER G.: Visualization of diffusion tensor data using evenly spaced streamlines. In *Vision, Modelling and Visualization (VMV)* (2005), pp. 79–86.
- [MSE*06] MERHOF D., SONNTAG M., ENDERS F., NIMSKY C., HASTREITER P., GREINER G.: Hybrid visualization for white matter tracts using triangle strips and point sprites. *IEEE Transactions on Visualization and Computer Graphics* 12, 5 (2006), 1181–1188.
- [MVvW05] MOBERTS B., VILANOVA A., VAN WIJK J. J.: Evaluation of fiber clustering methods for diffusion tensor imaging. In *IEEE Visualization* (2005), pp. 65–72.
- [OW05] O'DONNELL L., WESTIN C.-F.: White matter tract clustering and correspondence in populations. In *MICCAI* (2005).
- [PB07] PREIM B., BARTZ D.: *Visualization in Medicine.* Morgan Kaufmann, 2007.
- [PFK07] PETROVIC V., FALLON J., KUESTER F.: Visualizing whole-brain DTI tractography with GPU-based tuboids and LoD management. *IEEE Transactions on Visualization and Computer Graphics* 13, 6 (2007), 1488–1495.
- [SHWF98] SCOLLAN D., HOLMES A., WINSLOW R., FORDER J.: Histological validation of myocardial microstructure obtained from diffusion tensor magnetic resonance imaging. *American Journal of Physiology* 275 (1998), 2308–2318.
- [SM04] SCHUSSMAN G., MA K.-L.: Anisotropic volume rendering for extremely dense, thin line data. In *Proceedings of IEEE Visualization* (2004), pp. 107–114.
- [STS07] SCHULTZ T., THEISEL H., SEIDEL H.-P.: Topological visualization of brain diffusion mri data. *IEEE Transactions on Visualization and Computer Graphics* 13, 6 (2007), 1496–1503.
- [VBvP04] VILANOVA A., BERENSCHOT G., VAN PUL C.: DTI visualization with stream surfaces and evenly-spaced volume seeding. In *Eurographics/IEEE Symposium on Visualization* (2004), pp. 173–182.
- [WH06] WEICKERT J., HAGEN H.: *Visualization and Processing of Tensor Fields.* Springer, 2006.
- [WKZL04] WENGER A., KEEFE D., ZHANG S., LAIDLAW D. H.: Interactive volume rendering of thin thread structures within multivalued scientific datasets. *IEEE Transactions on Visualization and Computer Graphics* 10, 6 (2004), 664–672.
- [WSE07] WEISKOPF D., SCHAFFITZEL T., ERTL T.: Texture-based visualization of unsteady 3D flow by real-time advection and volumetric illumination. *IEEE Transactions on Visualization and Computer Graphics* 13, 3 (2007), 569–582.
- [ZCL08] ZHANG S., CORREIA S., LAIDLAW D. H.: Identifying white-matter fiber bundles in DTI data using an automated proximity-based fiber-clustering method. *IEEE Transactions on Visualization and Computer Graphics* (2008). In Press.
- [ZDL03] ZHANG S., DEMIRALP C., LAIDLAW D. H.: Visualizing diffusion tensor MR images using streamtubes and streamsurfaces. *IEEE Transactions on Visualization and Computer Graphics* 9, 4 (2003), 454–462.